Regular Article

On Performance Evaluation Of Hybrid Satellite-Terrestrial Relaying Networks With Fountain coding, NOMA and RIS

Nguyen Van Toan[1,4], Pham Ngoc Son[1], Tran Trung Duy[2], Lam-Thanh Tu[3], Ta Van-Thanh[4]

[1] Ho Chi Minh City University of Technology and Education, Ho Chi Minh City, Vietnam
[2] Posts and Telecommunications Institute of Technology, Ha Noi, Vietnam
[3] Advanced Intelligent Technology Research Group, Faculty of Electrical and Electronics Engineering, Ton Duc Thang University, Ho Chi Minh city, Vietnam
4 Telecommunications University, Khanh Hoa, Vietnam

Correspondence: Pham Ngoc Son, sonpndtvt@hcmute.edu.vn
Communication: received 08 August 2025, revised 11 September 2025, accepted 21 September 2025
Online publication: 22 September 2025, Digital Object Identifier: 10.21553/rev-jec.415

Abstract– **In this paper, we analyze outage probability (OP) of a hybrid satellite-terrestrial non-orthogonal multiple access (NOMA) relay system, where Fountain coding (FC) is used. In this system, Fountain-encoded packets are transmitted from the satellite to two terrestrial users. To assist the communication between a satellite and users, a reconfigurable intelligent surface (RIS) and a relay node are simultaneously utilized. To employ the advantages of the cooperative scheme, at the relay station, the fountain-encoded packets are decoded and then forwarded both directly without the RIS and indirectly with the RIS to the two users. We analyze the system's performance through theoretical analysis and propose a closed-form formula for the OP of both users over shadowing and Nakagami-m fading channels. Monte Carlo simulations confirm the correctness of the theoretical analysis by providing empirical evidence that supports the predicted outcomes under various scenarios and conditions. Additionally, factors influencing OP, such as satellite-terrestrial channel conditions, the number of reflecting elements in the RIS, FC parameters, and power allocation coefficients, are thoroughly investigated. Our findings demonstrate that integrating NOMA, RIS, and FC substantially improves system performance. Moreover, the results also reveal that to achieve the specified OP target, the system can dynamically adjust suitable power allocation coefficients for users, the number of elements in the reflector, or appropriate FC parameters.**

Keywords– **Hybrid Satellite–Terrestrial Relaying Networks (HSTRN), Non-Orthogonal Multiple Access (NOMA), Fountain coding (FC), Reconfigurable Intelligent Surface (RIS).**

1 Introduction

Recently, satellite communications have become an important part of the 6G mobile networks by offering robust line-of-sight (LOS) connections and large area coverage, which reduces the communication difficulties in remote and challenging terrains [1, 2]. In spite of the profound benefits of the communication links, one obstacle that may impede the development of satellite communication for applications such as long-range (LoRa) networks and remote sensors is their high expense [3, 4]. In order to maximize the benefits of satellite technology while dealing with cost concerns, a satellite-terrestrial network incorporating relaying techniques is a possible solution for low-cost devices [5, 6]. With the rapid development of HSTRN systems, many techniques have been introduced and applied, such as non-orthogonal multiple access (NOMA), reconfigurable intelligent surface (RIS), and Fountain coding (FC). These techniques offer several advantages for HSTRN systems, such as enhancing signal strength and quality through reflection, refraction, or diffraction. They significantly improve spectral efficiency compared to traditional orthogonal multiple access methods, and Fountain codes are highly effective for recovering lost or corrupted data.

1.1 Related Works

To deal with spectrum scarcity and ensure fairness among users, numerous studies have implemented NOMA techniques in HSTRN networks [7–14]. Specifically, [7] focused on analyzing the performance (outage probability and throughput) of the HSTRN system, in which the NOMA scheme was used. The authors in [7] highlighted the advantages of the NOMA scheme in enhancing spectrum utilization efficiency and analyzed the impact of interference among cells. The authors in [8] investigated the NOMA scheme in a satellite communication system, where the satellite directly transmits to the near user, who then acts as a relay node to forward signals to the far user. However, the authors in [9] introduced an HSTRN system using the NOMA scheme with multiple relays, where users act as relay nodes to enhance system performance. The work in [10] investigated the outage probability (OP) and average symbol error rate (ASER) in both perfect and imperfect successive interference cancellation (SIC) conditions for an HSTRN system. This system includes a satellite, a destination ground station (DGS), mobile users (CUs), and small base stations (SBSs), and operates based on

the NOMA scheme under co-channel interference (CCI) conditions. On the other hand, the authors in [11] proposed an uplink HSTRN (UL-HSTRN) system using the NOMA scheme with different priority users to enhance the signal transmission quality. To evaluate the system performance, accurate and approximate analytical OP expressions were provided based on ensuring signal transmission in a non-homogeneous channel environment, depending on the quality of service (QoS) of each user. In addition, the paper [12] investigates an HSTRN system based on NOMA under the influence of hardware impairments (HIs), using an opportunistic scheduling scheme to select the optimal relay node and the maximum ratio combination (MRC) technique to combine signals from the satellite with that relay. The authors derive closed-form expressions for the average SER for both far and near users, assuming HIs at all system nodes. In [13] and [14], the authors explored the cognitive radio approach for NOMA-HSTRN networks. Both studies focused on the performance of spectrum sharing in HSTRN systems, applying NOMA during the signal transmission phase at the ground station. It is worth noting that these studies focused solely on the NOMA-HSTRN system without considering the potential application of RIS. Additionally, there has been no exploration of the implementation of NOMA-HSTRN with FC techniques.

RIS can be dynamically reconfigured to adapt to changing network conditions or user demands. Thus, presently, there are several studies on HSTRN systems using RIS to improve the performance [15–17]. Specially in [15], a satellite transmits signals to multiple users through a relay station and a reflective surface. The authors combined beamforming and optimization techniques to reduce the total transmission power. The authors in [16] investigated a different scenario where a satellite transmits signals indirectly to users, experiencing significant signal blockage and path loss in the direct path. The authors in [17] utilized ground-installed RIS to aid the HSTRN system to reflect the signals to the user. The authors employed the amplify-and-forward (AF) protocol at the relay. However, the model overlooked the practical scenario where the destination user could receive direct signals from the relay in addition to the reflected signals via RIS. Furthermore, the authors conducted an analysis and derived closed-form expressions for the parameters OP, ergodic capacity, and SER of the RIS-assisted HSTRN system using the orthogonal multiple access (OMA) technique. Research has shown significant potential for integrating RIS into HSTRN systems. However, the application of FC and the NOMA scheme in these systems has not been considered.

FC well in scenarios, where data packets might be lost during transmission, such as in wireless networks or streaming applications. Moreover, FC is also inherent simplicity and low computational overhead, and low energy, size, memory costs. FCs can significantly reduce feedback latency and retransmission overhead [18–20]. Thus, the numerous studies have explored the application of FCs in various communication scenarios, demonstrating their effectiveness in improving system security, reliability, and efficiency [21–25]. In [21], the authors investigated the security performance of a multiple-input multiple-output (MIMO) system employing both NOMA and OMA schemes. The authors demonstrated that the combination of FCs and NOMA could reduce the required number of time slots by half compared to the OMA scheme. The work in [22] focused on evaluating the security of terrestrial networks using the low-energy adaptive clustering hierarchy (LEACH) protocol with FCs. The study delved into the trade-off between security probability and system reliability in the LEACH network, proposing accurate closed-form expressions for information privacy and OP. In [23], the authors examined the influence of FCs in cognitive radio broadcasting networks, while [24] investigated effects in ground-based networks with a multi-antenna access point transmitting Fountain encoded signals to multiple users. Works in [25] delved into an HSTRN scenario in which a satellite transmits rateless codes (a type of FC) to multiple users through the assistance of a relay station. The study analyzed the OP of both individual users and the entire system under the influence of CCI. However, the limitations of this work are the lack of closed-form analytical expressions and the absence of investigations on outage probabilities under different channel conditions.

1.2 Motivation and Contributions

Although extensive research has been conducted on communication within HSTRNs, several key aspects remain underexplored. For instance, studies in [7–14] have investigated HSTRN systems employing the NOMA technique. However, these works did not incorporate RIS into their models. Conversely, other studies have considered the integration of RIS in HSTRN networks [15–17], but without involving NOMA technology. In parallel, several works have explored the application of FC to improve the performance of terrestrial wireless communication systems [21–24].

Motivated by these advancements, recent studies have begun investigating NOMA–HSTRN systems that incorporate both FC and RIS. Notably, the authors in [26] proposed such a model and analyzed its secrecy performance. However, their system model presents some limitations. Specifically, it only considers an indirect transmission link from the relay to the user via RIS, neglecting practical scenarios in which the user may simultaneously receive signals through both direct and indirect paths. Furthermore, the study primarily focuses on physical layer security, while other critical performance metrics—such as outage behavior, throughput, and resource allocation—are not thoroughly addressed.

This research gap serves as the primary motivation for our focused investigation in this area. In this paper, we present an HSTRN model that integrates NOMA, RIS, and FC techniques, aiming to address the following key contributions:

- Firstly, we propose a model employing RIS and FC for the NOMA-HSTRN scheme to create a powerful and efficient communication system. Unlike previous works that only considered indirect RIS-assisted

links, our model allows each user to receive signals from the relay both directly and indirectly through the RIS, which reflects more practical deployment scenarios. Particularly, Fountain encoding is employed to address the issue of packet retransmission when users encounter errors, reducing system latency, and accommodating systems with unknown channel characteristics information (CCI). Receivers do not need to know the packet order but can still successfully decode the entire original message once they receive the minimum required number of encoded packets.

- Secondly, we analyze the impact of variations in the number of reflection elements and parameters related to Fountain encoding, such as the maximum number of sent packets (H_{max}) and the minimum number of received packets (G_{min}) required for decoding, on system performance evaluation metrics. We investigate the power allocation coefficient of users concerning the OP and identify the optimal parameters for the proposed system. In addition, different from most prior studies that assumed Rayleigh fading, our work considers Nakagami-m fading channels, thereby providing a more general and realistic performance evaluation. The results show that the combined RIS and FC can reduce both the OP and the system's transmission power requirements significantly.
- Thirdly, we derive closed-form expressions of the OP for each user to address challenges in practical satellite-terrestrial channels. This makes the relationships between variables more clearly and easier to understand, offering deeper insights into the system parameters. Moreover, we perform simulations to verify the convergence of the analytical results, thereby confirming the accuracy of the analytical formulas.

The rest of this paper is organized as follows. Section 2 presents the system model while section 3 derives the system performance in terms of outage probabilities. Section 4 presents the results and discussion, and section 5 is the conclusion.

2 System Model

We consider a downlink NOMA-HSTRN system, as illustrated in Figure 1. The system consists of a satellite (S) serving two terrestrial users (denoted as D_i with $i = 1, 2$ and utilizes a dedicated half-duplex Decode-and-Forward (DF) relay (denoted as R). Suppose that S, R, D_i are single-antenna devices and D_1 is assumed to be the far user while D_2 is the near user. Due to significant signal attenuation in the direct paths from the satellite to the users, the relay station is deployed to assist in decoding the satellite's transmissions. Subsequently, the processed signals are forwarded directly to the users and additionally reflected through a RIS (denoted as I) to enhance signal reception at the user terminals. At the satellite, the information intended for users D_i is divided into equally-sized packets, which are

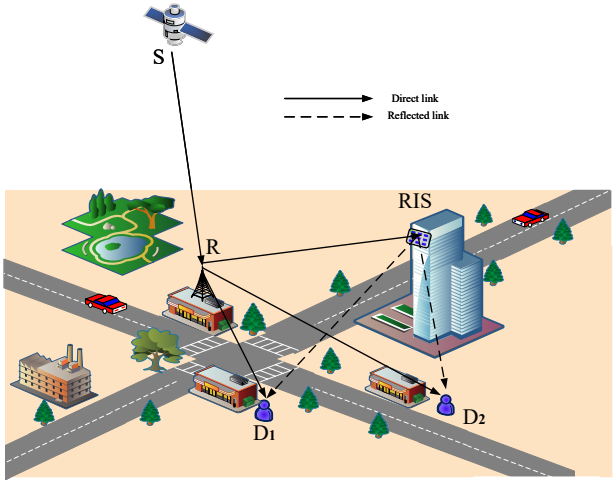

Figure 1. System Model.

then encoded using FC principles to generate packets for each user D_i [19]. The process of transmitting packets to users D_i is carried out in two phases: broadcast phase from S to R and terrestrial phase from R to D_i. At the R, perfect successive interference cancellation (pSIC) is applied to separate the signals intended for each user. Subsequently, FC is performed sequentially for users D_1 and D_2.

2.1 Broadcast Phase

In the first transmission phase, the source node S employs FC to divide the original message into equal-length data packets, and then encodes them into packets x_1 and x_2, intended for users D_1 and D_2, respectively [18, 20, 23]. By applying power-domain NOMA, the superimposed signal transmitted from S can be expressed as

$$x_S = \sqrt{a_1 P_S} x_1 + \sqrt{a_2 P_S} x_2, \tag{1}$$

where P_S and a_i are transmit power and power allocation coefficients of S, respectively. During this phase, the determination of a_1 and a_2 can be exchanged for each other, and we set $a_2 < a_1$ and $\sum_{i=1}^{2} a_i = 1$ [9]. The signal received at R is

$$y_R = \sqrt{a_1 P_S} h_{SR} x_1 + \sqrt{a_2 P_S} h_{SR} x_2 + n_R, \tag{2}$$

where $n_R \sim CN(0, \sigma_R^2)$ is the additive white Gaussian noise component (AWGN) at R with the mean zero and variance σ_R^2. The h_{SR} is channel coefficient from S to R, which belongs the shadowed-Rician distribution [10].

Moreover, in order to consider the impacts of satellite beam gain and path loss h_{SR} [9, Equation (25)], we can model the channel coefficient as

$$h_{SR} = Q_{SR} g_{SR}, \tag{3}$$

herein, $Q_{SR} = \frac{c\sqrt{G_{SR}\theta_{SR}}}{4\pi f_c^S d_{SR}}$, with c is the speed of light, f_c^S is the carrier frequency, d_{SR} is the distance from the satellite to the terrestrial relay R, and $G_{SR}\theta_{SR}$ is the beam gain. The beam gain is given by $G_{SR}\theta_{SR} = G_{SR}^{max}\left(\frac{J_1(u_{SR})}{2u_{SR}} + 36\frac{J_3(u_{SR})}{u_{SR}^3}\right)$ with G_{SR}^{max} being the

maximum satellite beam gain and $u_{\mathrm{SR}} = \frac{2.071223 \sin\theta_{\mathrm{SR}}}{\sin\theta_{3dB}}$, where θ_{SR} is the angle between the terrestrial receiver R and the beam center in relation to the satellite, and θ_{3dB} is the fixed 3-dB angle for the beam. To achieve optimal system performance, as shown in [14, 27], we set $\theta_{\mathrm{SR}} \to 0$, result in $h_{\mathrm{SR}} = Q_{\mathrm{SR}}^{\max} g_{\mathrm{SR}}$, where $Q_{\mathrm{SR}}^{\max} = \frac{c\sqrt{G_{\mathrm{SR}}^{\max}}}{4\pi f_c^S d_{\mathrm{SR}}}$ is the maximum scaling coefficient characterizing the propagation loss. Additionally, the S-R channel coefficient gain $|g_{\mathrm{SR}}|^2$ follows the Rician shadowing distribution in which its probability density function (PDF) is determined by equation (4), as follows [8–10]

$$f_{|g_{\mathrm{SR}}|^2}(x) = \frac{1}{2b}\Big(\frac{2ab}{2ab+\Omega}\Big)^a \exp\Big(-\frac{x}{2b}\Big) \times {}_1F_1\Big(a;1;\frac{\Omega x}{2b(2ab+\Omega)}\Big). \quad (4)$$

In (4), Ω is the average power of the LOS between S and R, $2b$ is the average value of the multipath component S - R, m is a characteristic parameter for the Nakagami channel, and ${}_1F_1(.;..;..)$ is the confluent hypergeometric function [28]. We have the instantaneous Signal-to-Interference-plus-Noise Ratio (SINR) at R to decode the signals x_1 and x_2, respectively, as follows:

$$\gamma_{\mathrm{R}}^{x_1} = \frac{P_{\mathrm{S}} a_1 |h_{\mathrm{SR}}|^2}{P_{\mathrm{S}} a_2 |h_{\mathrm{SR}}|^2 + \sigma_{\mathrm{R}}^2} = \frac{P_{\mathrm{S}} a_1 |Q_{\mathrm{SR}}^{\max} g_{\mathrm{SR}}|^2}{P_{\mathrm{S}} a_2 |Q_{\mathrm{SR}}^{\max} g_{\mathrm{SR}}|^2 + \sigma_{\mathrm{R}}^2} = \frac{\Lambda a_1 (Q_{\mathrm{SR}}^{\max})^2 X}{\Lambda a_2 (Q_{\mathrm{SR}}^{\max})^2 X + 1}, \quad (5)$$

and

$$\gamma_{\mathrm{R}}^{x_2} = \Lambda a_2 (Q_{\mathrm{SR}}^{\max})^2 X, \quad (6)$$

where $\Lambda = \frac{P_{\mathrm{S}}}{\sigma_{\mathrm{R}}^2}$ and $X = |g_{\mathrm{SR}}|^2$.

2.2 Terrestrial Phase

At R relay uses Fountain coding to encode the data transmitted to the users D_i. R employs the superimposed coding (SC) technique with power allocation coefficients b_1 and b_2 for D_1, and D_2, respectively, with $b_1 > b_2$ and $b_1 + b_2 = 1$. The signal transmitted at R is

$$x_{\mathrm{R}} = \sqrt{b_1 P_{\mathrm{R}}} x_1 + \sqrt{b_2 P_{\mathrm{R}}} x_2. \quad (7)$$

The signal received at D_i is given by [29]

$$y_{\mathrm{D}_i} = (h_{\mathrm{RD}_i} + \sum_{n=1}^{N} h_{\mathrm{RI}_n} h_{\mathrm{I}_n\mathrm{D}_i} e^{-j\theta_n}) x_{\mathrm{R}} + n_{\mathrm{D}i}. \quad (8)$$

In (8), $P_{\mathrm{R}} = \mu P_{\mathrm{S}}$ is transmit power of R, which μ is the ratio coefficient between the transmit power of S and the transmit power of R and $0 < \mu \leq 1$. θ_n is phase shift of the n^{th} RE of RIS, $n_{\mathrm{D}i} \sim CN(0, \sigma_{\mathrm{Di}})$ is the Gaussian noise at D_i. On the other hand, since Θ is a complex variable, it can be expressed as $h_{\mathrm{RD}_i} = |h_{\mathrm{RD}_i}| e^{-j\theta_{\mathrm{RD}_i}}$, $h_{\mathrm{RI}_n} = |h_{\mathrm{RI}_n}| e^{-j\theta_{\mathrm{RI}_n}}$, and $h_{\mathrm{I}_n\mathrm{D}_i} = |h_{\mathrm{I}_n\mathrm{D}_i}| e^{-j\theta_{\mathrm{I}_n\mathrm{D}_i}}$, where $|h_{\mathrm{RD}_i}|$, $|h_{\mathrm{RI}_n}|$, and $|h_{\mathrm{I}_n\mathrm{D}_i}|$ are the magnitudes, and θ_{RD_i}, θ_{RI_n}, and $\theta_{\mathrm{I}_n\mathrm{D}_i}$ are the phases of h_{RD_i}, h_{RI_n}, and $h_{\mathrm{I}_n\mathrm{D}_i}$, respectively. We consider the R- $\mathrm{D_i}$ channels are Nakagami-m - fading terrestrial channels, thus PDF and CDF of the magnitude Θ are given by

$$f_\Theta(x) = \frac{2m_\Theta^{m_\Theta}}{\Gamma(m_\Theta)\Omega_\Theta^{m_\Theta}} x^{2m_\Theta - 1} \exp(-\frac{m_\Theta}{\Omega_\Theta} x^2),\ x \geq 0, \quad (9)$$

$$F_\Theta(x) = \frac{1}{\Gamma(m_\Theta)} \gamma(m_\Theta, \frac{m_\Theta}{\Omega_\Theta} x^2) = 1 - \frac{1}{\Gamma(m_\Theta)} \Gamma(m_\Theta, \frac{m_\Theta}{\Omega_\Theta} x^2),\ x \geq 0, \quad (10)$$

where m_Θ and Ω_Θ are the shape and spread parameters respectively. According to [29], Ω_Θ is calculated as

$$\Omega_\Theta = G_{pq} - 22.7 - 26\log(f_c^{\mathrm{PQ}}) - 36.7\log(d_{\mathrm{PQ}}) + G_{cq}, \quad (11)$$

where G_{pq} and G_{cq} are the antenna gains of the transmitter and receiver respectively, the carrier frequency is $2 \leq f_c^{\mathrm{PQ}} \leq 6$ GHz, and d_{PQ} ($\mathrm{PQ} \in \mathrm{RD}_i, \mathrm{RI}_n, \mathrm{I}_n\mathrm{D}_i$) is the distance from the transmitter to the receiver. Based on the aforementioned magnitudes and phases, the received signal at D_i can be expressed as

$$y_{\mathrm{D}_i} = e^{-j\theta_{\mathrm{RD}_i}} \Bigg(|h_{\mathrm{RD}_i}| + \sum_{n=1}^{N} |h_{\mathrm{RI}_n}||h_{\mathrm{I}_n\mathrm{D}_i}| \times e^{j(\theta_n - \theta_{\mathrm{RI}_n} - \theta_{\mathrm{I}_n\mathrm{D}_i} + \theta_{\mathrm{RD}_i})} \Bigg) \sum_{i=1}^{2} \sqrt{b_i P_{\mathrm{R}}} x_i + n_{\mathrm{D}_i}, \quad (12)$$

where $\theta_n - \theta_{\mathrm{RI}_n} - \theta_{\mathrm{I}_n\mathrm{D}_i} + \theta_{\mathrm{RD}_i}$ is considered the phase error of the n^{th} RE of RIS. Similar to the approach in [29], and under the assumption of perfect channel state information (CSI), the optimization with respect to the phase satisfies $\theta_n - \theta_{\mathrm{RI}_n} - \theta_{\mathrm{I}_n\mathrm{D}_i} + \theta_{\mathrm{RD}_i} = 0$. Hence, we obtain

$$y_{\mathrm{D}_i} = e^{-j\theta_{\mathrm{RD}_i}} \Bigg(|h_{\mathrm{RD}_i}| + \sum_{n=1}^{N} |h_{\mathrm{RI}_n}||h_{\mathrm{I}_n\mathrm{D}_i}| \Bigg) \sum_{i=1}^{2} \sqrt{b_i P_{\mathrm{R}}} x_i + n_{\mathrm{D}_i}. \quad (13)$$

Then, the SINRs at D_1 to decode the signal x_1, at D_2 to decode two signals x_1 and x_2, as follows

$$\gamma_{\mathrm{D}_1}^{x_1} = \frac{\mu\Lambda b_1 \Big(|h_{\mathrm{RD}_1}| + Z_1\Big)^2}{\mu\Lambda b_2 \Big(|h_{\mathrm{RD}_1}| + Z_1\Big)^2 + 1} = \frac{\mu\Lambda b_1 |v_{\mathrm{RD}_1}|^2}{\mu\Lambda b_2 |v_{\mathrm{RD}_1}|^2 + 1}, \quad (14)$$

where $Z_1 = \sum_{n=1}^{N} |h_{\mathrm{RI}_n}||h_{\mathrm{I}_n\mathrm{D}_1}|$, $v_{\mathrm{RD}_1} = |h_{\mathrm{RD}_1}| + Z_1$ and $\Lambda = \frac{P_{\mathrm{S}}}{\sigma_0^2}$. Similarly, we obtain

$$\gamma_{\mathrm{D}_2}^{x_1} = \frac{\mu\Lambda b_1 |v_{\mathrm{RD}_2}|^2}{\mu\Lambda b_2 |v_{\mathrm{RD}_2}|^2 + 1}, \quad (15)$$

$$\gamma_{\mathrm{D}_2}^{x_2} = \mu\Lambda b_2 (|h_{\mathrm{RD}_2}| + Z_2)^2 = \mu\Lambda b_2 |v_{\mathrm{RD}_2}|^2, \quad (16)$$

where $Z_2 = \sum_{n=1}^{N} |h_{\mathrm{RI}_n}||h_{\mathrm{I}_n\mathrm{D}_2}|$ and $v_{\mathrm{RD}_2} = |h_{\mathrm{RD}_2}| + Z_2$.

Remark 1: *When considering the case of the proposed system model without RIS, the signal in the terrestrial phase is transmitted directly from R to users D_i, $i = 1, 2$. Then, $Z_i = 0$ in the formulas* (14), (15), (16).

Decoded signals at R then is re-encoded and forwarded in two directions, directly to D_i and indirectly through RIS to D_i. Thus, the end-to-end SINRs at users D_i are defined as

$$\gamma_{D_1}^{e2e} = \min(\gamma_R^{x1}, \gamma_{D_1}^{x1}),$$
$$\gamma_{D_2}^{e2e} = \min(\gamma_R^{x_1}, \gamma_R^{x_2}, \gamma_{D_2}^{x_1}, \gamma_{D_2}^{x_2}). \quad (17)$$

In (17), $\gamma_{D_1}^{e2e}$ is donated by the weaker of the decoding processes at the relay and at D_1, since only x_1 is decoded without SIC. Meanwhile, $\gamma_{D_2}^{e2e}$ is determined by the minimum SINR required for decoding x_1 and x_2 at both R and D_2, due to the use of SIC.

3 Outage Probability

Outage probability (OP) is defined as the probability that the instantaneous channel capacity is below a predetermined threshold.

3.1 Decoding of one encoded packet at D_i

The decoding process at user D_i is considered unsuccessful under two conditions: either the decoding fails at R, or the decoding succeeds at R but then fails at D_i. The probability formula for decoding failure of a FC package at D_i is

$$P_{D_i} = \Pr\left(\log_2(1 + \gamma_{Di}^{e2e}) < C_{th}\right), \quad (18)$$

where $\gamma_{D_i}^{e2e}$ is defined by (17) and C_{th} is threshold speed. Let $\gamma_{th} = 2^{C_{th}} - 1$, (18) can be rewritten as

$$P_{D_i} = \Pr\left(\gamma_{Di}^{e2e} < \gamma_{th}\right). \quad (19)$$

Replacing (17) into (19), we have P_{D_1} and P_{D_2} as follows

$$P_{D_1} = \Pr\left(\min(\gamma_R^{x_1}, \gamma_{D_1}^{x_1}) < \gamma_{th}\right),$$
$$P_{D_2} = \Pr\left(\min(\gamma_R^{x_1}, \gamma_R^{x_2}, \gamma_{D_2}^{x_1}, \gamma_{D_2}^{x_2}) < \gamma_{th}\right). \quad (20)$$

From (20), we can calculate P_{D_i} of the proposed system are presented in Theorem 1 and Theorem 2.

Theorem 1: The unsuccessful decoding of one encoded packet of user D_1 is given as

$$P_{D_1} = T_1 + T_2 - T_1 \times T_2, \quad (21)$$

where T_1 and T_2 are given as in (22) and (23) at the top of the next page, respectively.

Proof: Please see Appendix A.

Theorem 2: Unsuccessful decoding of one encoded packet of user D_2 in the proposed system is obtained as

$$P_{D_2} = T_3 + T_4 - T_3 \times T_4, \quad (24)$$

where T_3 and T_4 are given as in (25) and (26) at the top of the next page, respectively.

Proof: Please see Appendix B.

Remark 2: *Considering the model without RIS (WoRIS) support for the transmission in the terrestrial phase. The probabilities of unsuccessful decoding of an encoded packet, P_{D_1} and P_{D_2}, are determined as*

$$P_{D_1} = \Pr\left(\min(\gamma_R^{x_1}, \gamma_{D_1}^{x_1}) < \gamma_{th}\right)$$
$$P_{D_2} = \Pr\left(\min(\gamma_R^{x_1}, \gamma_R^{x_2}, \gamma_{D_2}^{x_1}, \gamma_{D_2}^{x_2}) < \gamma_{th}\right). \quad (27)$$

In (27), P_{D1} and PD_2 denote the OPs of D_1 and D_2, respectively. The SINR values at R and D_i in the WoRIS model are computed in the same manner as in the RIS-assisted model (WiRIS), except that the contribution of the indirect link R–RIS–D_i is set to zero. This ensures a fair performance comparison between the two schemes.

3.2 Outage Probability at D_1 and D_2

From the calculating in subsection 3.1, P_{D_i} is the probability of unsuccessful decoding of one encoded packet at user D_i, while $1 - P_{D_i}$ is the probability of successfully decoding one encoded packet. Let r_{D_i} is the number of encoded packets that can accurately receive. In the case of $r_{D_i} < G_{\min}$, D_i is unable to retrieve the satellite's data. Consequently, the OP at D_i can be determined as

$$\mathrm{OP}_i = \sum_{r_{D_i}=0}^{G_{\min}-1} \binom{H_{\max}}{r_{D_i}} (1 - P_{D_i})^{r_{D_i}} (P_{D_i})^{H_{\max} - r_{D_i}}, \quad (28)$$

where $\binom{H_{max}}{r_{D_i}} = \dfrac{H_{max}!}{r_{D_i}!(H_{\max} - r_{D_i})!}$, G_{min} is the minimum number of encoded packets received successfully at D_i, and H_{max} is the maximum number of encoded packets sent by the transmitter.

4 Numerical Results and Discussion

This section we provide the numerical results of the considered system. The channel coefficient from S to R follows the Shadowed Rician model, while the channel coefficients between R and D_i is Nakagami-m. Simulations are conducted by 10^6 samples with parameters presented in Table I and Table II. The locations of R, RIS (I), and D_i are setting in three-dimensional (3D) parameters, specifically $(x_R, y_R, z_R), (x_I, y_I, z_I), (x_{D_i}, y_{D_i}, y_{D_i})$. Accordingly, the distances between the nodes are $d_{PQ} = \sqrt{(z_P - z_Q)^2 + (y_P - y_Q)^2 + (x_P - x_Q)^2}$ with $P, Q \in (R, I, D_i)$ and $P \neq Q$. The shape parameter $m_\Theta = 3$ and the spread parameter Ω_Θ are determined according to (11). The parameters G_{pq} and G_{cq} are choose as [30] and [31].

Table I
Shadowing Rician Channel Parameters [3, 9]

Shadowing	a	b	Ω
Frequent heavy shadowing (FHS)	0.739	0.063	0.0007
Average shadowing (AS)	5.1	0.251	0.279

Figure 2 examined the accuracy of the approximated OP expressions versus Chebyshev parameter in the case of $P_S = 25$ dB, Fountain encoding parameters $H_{max} = 6$ and $G_{min} = 4$. Using equations (34), (42) and (44), OP

$$T_1 = \begin{cases} 1; \frac{a_1}{a_2} \leq \gamma_{\text{th}} \\ \zeta_A \sum\limits_{m=1}^{M} \frac{\sqrt{1-\phi_m^2}}{2b} \exp\left(-\frac{A}{4b}(1+\phi_m)\right) {}_1F_1\left(a, 1, \frac{\Omega A(1+\phi_m)}{4b(2ab+\Omega)}\right); \frac{a_1}{a_2} > \gamma_{\text{th}} \end{cases} \tag{22}$$

$$T_2 = \begin{cases} 1; \frac{b_1}{b_2} \leq \gamma_{th} \\ 1 - \frac{1}{\Gamma(\Xi_{\text{RD}_1})} \Gamma\left(\Xi_{\text{RD}_1}, \Delta_{\text{RD}_1} \sqrt{\frac{\gamma_{th}}{\mu\Lambda(b_1 - b_2\gamma_{th})}}\right); \frac{b_1}{b_2} > \gamma_{th} \end{cases} \tag{23}$$

$$T_3 = \begin{cases} 1; \frac{a_1}{a_2} < \gamma_{th} \\ \zeta_B \sum\limits_{m=1}^{M} \frac{\sqrt{1-\phi_m^2}}{2b} \exp\left(-\frac{B}{4b}(1+\phi_m)\right) {}_1F_1\left(a, 1, \frac{\Omega B(1+\phi_m)}{4b(2ab+\Omega)}\right); \frac{a_1}{a_2} > \gamma_{th} \geq \frac{a_1 - a_2}{a_2} \\ \zeta_C \sum\limits_{m=1}^{M} \frac{\sqrt{1-\phi_m^2}}{2b} \exp\left(-\frac{C}{4b}(1+\phi_m)\right) {}_1F_1\left(a, 1, \frac{\Omega C(1+\phi_m)}{4b(2ab+\Omega)}\right); \frac{a_1 - a_2}{a_2} > \gamma_{th} > 0 \end{cases} \tag{25}$$

$$T_4 = \begin{cases} 1; \frac{b_1}{b_2} \leq \gamma_{th} \\ 1 - \frac{1}{\Gamma(\Xi_{RD_2})} \Gamma\left(\Xi_{RD_2}, \Delta_{RD_2} \sqrt{\frac{\gamma_{th}}{\mu\Lambda b_2 \gamma_{th}}}\right); \frac{b_1}{b_2} > \gamma_{th} \geq \frac{b_1 - b_2}{b_2} \\ 1 - \frac{1}{\Gamma\left(\Xi_{RD_2}\right)} \Gamma\left(\Xi_{RD_2}, \Delta_{RD_2} \sqrt{\frac{\gamma_{th}}{\mu\Lambda(b_1 - b_2\gamma_{th})}}\right); \frac{b_1 - b_2}{b_2} > \gamma_{th} > 0 \end{cases} \tag{26}$$

Table II
System Parameters [7–9, 23, 27]

Parameters	Value
Satellite orbit type	LEO
Carrier frequency of satellite f_c^{SR}	1 GHz
3–dB angle θ_{3dB}	0.3°
Maximal satellite beam gain $G_{\max}$	48 dB
Receiving distance from satellite d_{SR}	3000 km
$a_1 = b_1$	0.85
$a_2 = b_2$	0.15
μ	1
Threshold rate C_{th}	1 bit per channel use (BPCU)
f_c^{PQ}	3 GHz
$(x_{\text{R}}, y_{\text{R}}, z_{\text{R}})$	$(100, 20, 100)$ m
$(x_{\text{I}}, y_{\text{I}}, z_{\text{I}})$	$(150, 20, 40)$ m
$(x_{\text{D}_1}, y_{\text{D}_1}, z_{\text{D}_1})$	$(230, 5, 0)$ m
$(x_{\text{D}_2}, y_{\text{D}_2}, z_{\text{D}_2})$	$(200, 10, 0)$ m

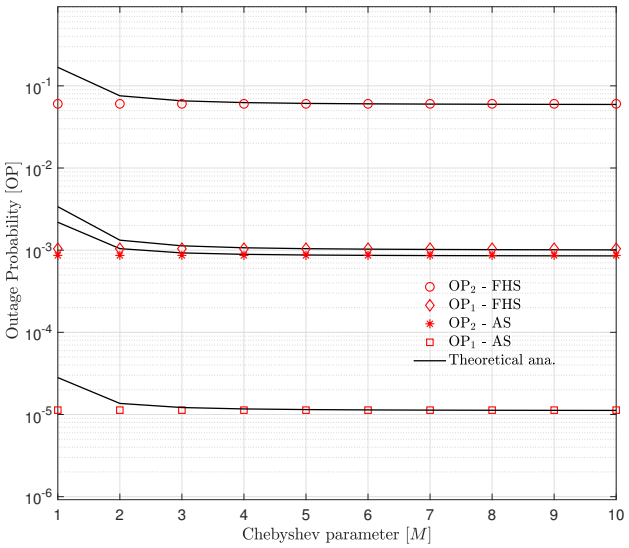

Figure 2. Survey of Chebyshev parameter selection.

analysis for user D_i is conducted via the Chebyshev integral expansion method. Unlike previous works on the HSTRN system model, this paper employs the Chebyshev integral expansion method, which facilitates the derivation of closed-form OP expressions. In this method, M is the Chebyshev parameter that determines the precision of the integral expansion. Figure 2 demonstrates that selecting $M > 3$ results the OP values to the saturation region, validating the accuracy of the expression transformation employed in this research. Therefore, the following simulations are all conducted with $M = 5$.

Figure 3 presents the comparison of OP versus average SNR for the proposed scheme across various shadowing scenarios. In this scheme, we consider $N = 80$ on the RIS. For a fair comparison, the channel model from R to D_i and all system parameters are kept identical between the WoRIS scheme and the WiRIS scheme. Therefore, the performance evaluation between the two models ensures fairness. The simulation results align well with the analytical findings shown in the figure, confirming the accuracy of our closed-form expressions (28) for OP derivation. Furthermore, it is evident that the RIS-assisted HSTRN system exhibits superior OP performance compared to the system without RIS in all shadowing scenarios.

Figure 4 examines the OP versus SNR with parameters as in Figure 3, showcasing the advantages of the proposed FC-HSTRN model with NOMA compared to the FC-HSTRN model with OMA. The graph indicates that the system employing NOMA with a reasonable power allocation factor significantly achieves higher performance. Specifically, under FHS channel conditions

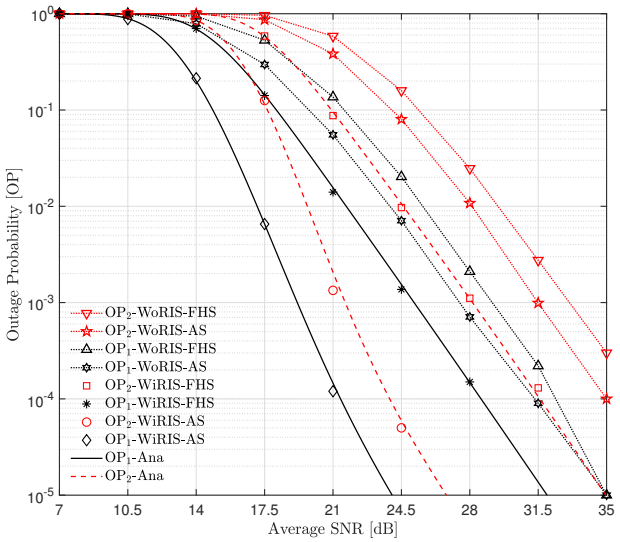

Figure 3. OP versus SNR with and without the RIS model when $H_{\max} = 6$, $G_{\min} = 4$.

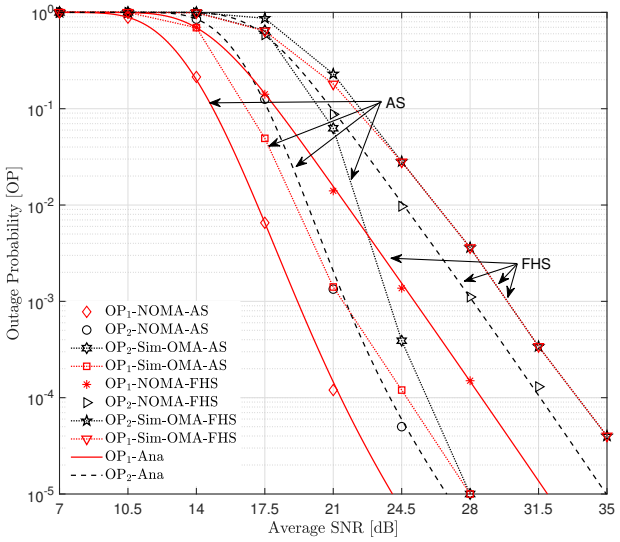

Figure 4. OP versus SNR with NOMA and OMA models when $H_{\max} = 6$, $G_{\min} = 4$.

at SNR = 28 dB, the OP for D_1 and D_2 in the NOMA combined system are 1.4×10^{-4} and 10^{-3}, respectively, while in the OMA system, their outage probabilities are both 0.36×10^{-2}. When the OP target is 10^{-3}, the required transmit power is only 25 dB and 28 dB with NOMA, whereas the OMA system requires a transmit power of up to 31.5 dB for both users. In other words, using NOMA significantly reduces the transmit power of S and R in the HSTRN system with FC. The graph also shows that at high SNR levels, the OP for both users in the OMA system converges, which is due to users having the same power level at the transmitter and being unaffected by interference from other receivers at high SNRs.

Both Figures 3 and 4 show that the OP values achieved for users D_1 and D_2 under AS channel conditions are always better than those under FHS conditions. Specifically, for the same OP target of 10^{-4}, the corresponding SNRs are 21.4 dB and 23.8 dB with AS, but 28.5 dB and 31.6 dB with FHS. This aligns with the reality that AS channel conditions are better than FHS channel conditions. The simulation results match the analytical results shown in Figures 3 and 4, confirming the accuracy of our closed-form expression for outage probabilities.

Figure 5 investigates the OP versus SNR while varying Fountain encoding parameters with $H_{\max} = 6$, $G_{\min} = 5, 4, 3$. The experiments are conducted with $N = 100$ reflectors under both AS channel conditions in Figure 5(a) and FHS conditions in Figure 5(b). In both figures, it is observed that decreasing $G_{\min}$ leads to a significant reduction in the OP values. Specifically, in Figure 5(a), at SNR = 17 dB, corresponding to $G_{\min} = 5, 4$, and 3, the values of OP_1 are 2.4×10^{-2}, 1.4×10^{-3}, and 4.3×10^{-5} respectively. The values of OP_2 are 2.6×10^{-1}, 5.8×10^{-1}, and 7.2×10^{-2}. This is explained by the fact that as $G_{\min}$ decreases, the probability of successful packet decoding increases, leading to a decrease in the OP. As mentioned in [19], varying $G_{\min}$ means changing the degree of encoding, where a lower degree implies increased complexity in the Fountain encoding and decoding process. Therefore, to achieve the desired OP, the system needs to select an appropriate degree of Fountain encoding. Through this investigation, it can be seen that the FC parameters significantly improve user performance; however, a trade-off between the OP and the encoding/decoding complexity must be considered.

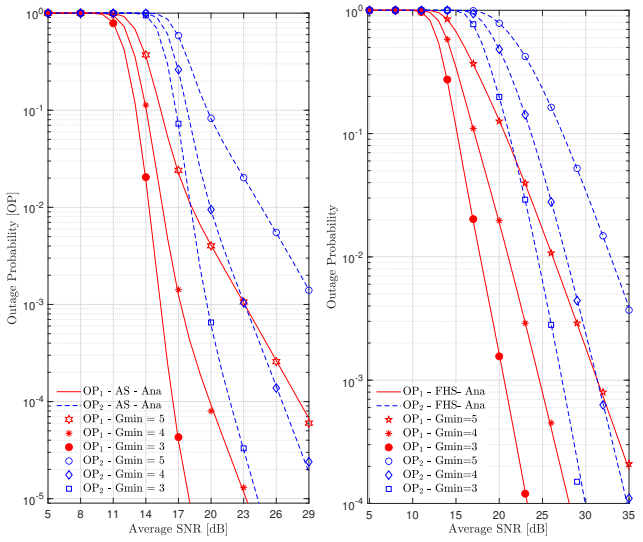

(a) AS channel (b) FHS channel

Figure 5. OP versus SNR with varying Fountain coding parameters.

Figure 6 investigates the impact of the power allocation coefficient a_1 on the OPs with parameters $P_S = 20$ dB and $N = 120$ under AS channel conditions. This figure demonstrates that with an increase in a_1, OP_1 decreases sharply, and OP_2 decreases to a minimum before increasing again. This occurs because as a_1 increases, the energy allocated to D_1 increases while the energy allocated to D_2 decreases. This study also indicates that when $a_1 = 0.67$, both OP_1 and OP_2 are equal, representing the optimal point of the system. At this point, the trade-off between the two users is

balanced: increasing a_1 enhances the reliability of D_1 but reduces that of D_2, and vice versa. Therefore, the intersection at $a_1 = 0.67$ corresponds to a fairness point where both users achieve equal performance, providing a useful guideline for practical power allocation design.

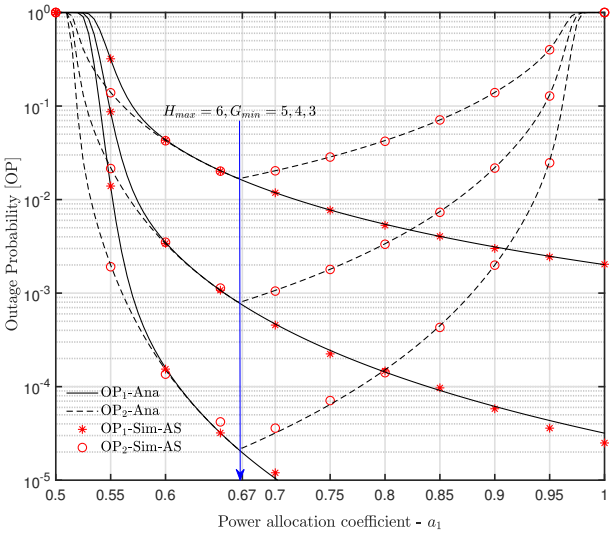

Figure 6. OP versus power allocation factor with varying FC parameters.

Figure 7 illustrates the impact of the number of elements in the reflector array on system performance with parameters $H_{\max} = 6$, $G_{\min} = 4$. The graph shows that increasing N improves system performance under AS channel conditions more than under FHS conditions. Specifically, at SNR = 15 dB, the value of OP_1 under AS channel conditions is 2.4×10^{-1} with $N = 80$ and 2×10^{-3} with $N = 120$, while OP_2 is 1.1×10^{-1} and 0.9, respectively. The graph also indicates that at high SNRs, OP_1 and OP_2 tend to converge. This is explained by the system using NOMA combined with FC, which increases the probability of successful decoding for both users D_1 and D_2 equivalently.

Figure 8 presents the survey results with $N = 100$, $H_{\max} = 6$, and $G_{\min} = 4$. The graph shows how the OP varies with the shape parameter of the Nakagami channel. When m is low, the OP is heavily influenced by the quality of the satellite transmission channel. As m increases, the OP improves significantly and eventually saturates. This saturation can be explained by formulas (21) and (24). When T_2 and T_4 are very small, the OP is primarily determined by T_1 and T_3, which are not affected by the parameter m.

5 Conclusion

This paper analyzed the outage performance of a HSTRN, FC, NOMA, and RIS. Closed-form outage probability expressions were derived for both users over shadowed Rician and Nakagami-m fading channels. The analytical results were verified through extensive Monte Carlo simulations, confirming the accuracy of the proposed framework. The results demonstrate that jointly employing FC, RIS, and NOMA significantly reduces

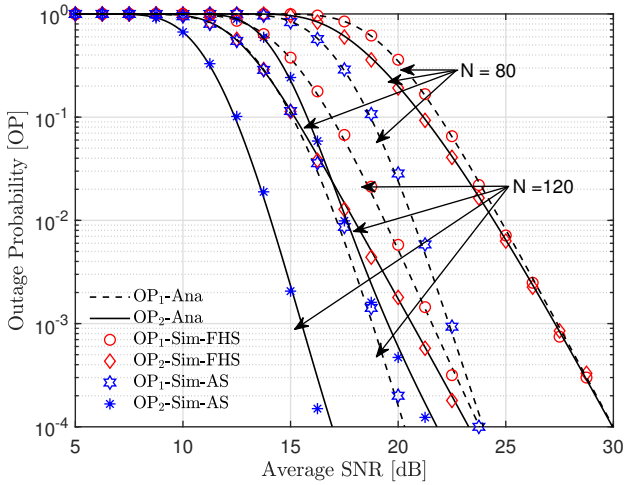

Figure 7. OP versus SNR with varying number of reflecting elements.

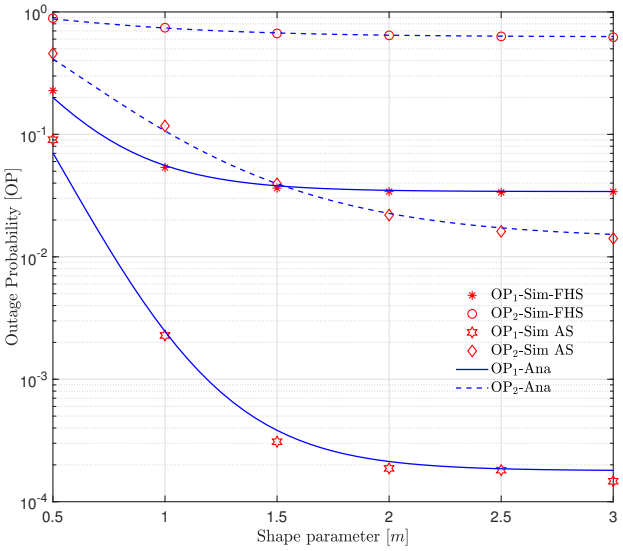

Figure 8. OP versus shape parameter of the Nakagami channel.

the outage probability and transmit power requirements compared with conventional HSTRN schemes. Furthermore, RIS configuration and FC parameter optimization provide additional degrees of freedom to balance reliability and decoding complexity, while proper power allocation improves fairness among users. From a practical perspective, the proposed design enables adaptive adjustment of RIS phases, coding parameters, and power allocation strategies to meet diverse QoS requirements with low energy consumption, making it highly suitable for next-generation non-terrestrial networks serving IoT and broadband applications. Future research will focus on the impact of imperfect CSI, residual hardware impairments, and direct satellite–user links. Moreover, energy-efficient designs and multi-RIS deployments will be explored to further enhance network performance and scalability.

Acknowledgements

This research is funded by Vietnam National Foundation for Science and Technology Development (NAFOSTED) under grant number 102.04-2021.57.

Appendix A

This appendix A is used to provide the detailed proof of theorem 1. Considering at R, the unsuccessful probability to receive one packet from S at the user D_1 is calculated as

$$\begin{aligned} P_{D_1} &= \Pr\left(\min(\gamma_R^{x_1}, \gamma_{D_1}^{x_1}) < \gamma_{th}\right) \\ &= \Pr(\gamma_R^{x_1} < \gamma_{th}) + \Pr(\gamma_{D_1}^{x_1} < \gamma_{th}) \\ &- \Pr(\gamma_R^{x_1} < \gamma_{th}) \times \Pr(\gamma_{D_1}^{x_1} < \gamma_{th}) \\ &= T_1 + T_2 - T_1 \times T_2. \end{aligned} \tag{29}$$

We can calculate T_1 as

$$T_1 = \Pr(\gamma_{R_1}^{x_1} < \gamma_{th}). \tag{30}$$

By replacing (5) into (30), we have

$$\begin{aligned} T_1 &= \Pr\left(\frac{\Lambda a_1 (Q_{SR}^{\max})^2 X}{\Lambda a_2 (Q_{SR}^{\max})^2 X + 1} < \gamma_{th}\right) \\ &= \Pr((a_1 - a_2\gamma_{th})(Q_{SR}^{\max})^2 \Lambda X < \gamma_{th}). \end{aligned} \tag{31}$$

It is noted that, in the case of $a_1 - a_2\gamma_{th} < 0$ the probability in (31), always occur. Therefore,

$$T_1 = \Pr((a_1 - a_2\gamma_{th})(Q_{SR}^{\max})^2 \Lambda X < \gamma_{th}) = 1. \tag{32}$$

On the other hand if $a_1 - a_2\gamma_{th} > 0$, because X has PDF according to (4), so the CDF of X is defined as (33)

$$\begin{aligned} T_1 = F_X(x) = \int_0^A \frac{1}{2b}\left(\frac{2ab}{2ab+\Omega}\right)^a \exp\left(-\frac{x}{2b}\right) \\ \times {}_1F_1\left(a; 1; \frac{\Omega x}{2b(2ab+\Omega)}\right) dx, \end{aligned} \tag{33}$$

where $A = \dfrac{\gamma_{th}}{(a_1 - a_2\gamma_{th})(Q_{SR}^{\max})^2 \Lambda}$. After applying the approximated Chebyshev-Gauss quadrature [32, Equation (25.4.30)], T_1 is rewritten as

$$T_1 = \begin{bmatrix} \dfrac{A\pi}{2M} \sum\limits_{m=1}^{M} \dfrac{\sqrt{1-\phi_m^2}}{2b}\left(\dfrac{2ab}{2ab+\Omega}\right)^a \\ \times \exp\left(-\dfrac{A}{4b}(1+\phi_m)\right) {}_1F_1\left(a, 1, \dfrac{\Omega A(1+\phi_m)}{4b(2ab+\Omega)}\right) \end{bmatrix}, \tag{34}$$

where M is Chebyshev parameter, $\phi_m = \cos\left(\dfrac{(2m-1)\pi}{2M}\right)$ and $\zeta_A = \frac{A\pi}{2M}\left(\dfrac{2ab}{2ab+\Omega}\right)^a$. Combining (32) and (34), we obtain T_1 as given in (22).

Similarly, we can formulate T_2 as in (35):

$$\begin{aligned} T_2 &= \Pr(\gamma_{D_1}^{x_1} < \gamma_{th}) = \Pr\left(\frac{\mu\Lambda b_1 |v_{RD_1}|^2}{\mu\Lambda b_2 |v_{RD_1}|^2 + 1} < \gamma_{th}\right) \\ &= \Pr(\mu\Lambda(b_1 - b_2\gamma_{th})|v_{RD_1}|^2 < \gamma_{th}) \\ &= \begin{cases} 1, & \dfrac{b_1}{b_2} \le \gamma_{th}, \\ F_{|v_{RD_1}|}\left(\sqrt{\dfrac{\gamma_{th}}{\mu\Lambda(b_1 - b_2\gamma_{th})}}\right), & \dfrac{b_1}{b_2} > \gamma_{th}. \end{cases} \end{aligned} \tag{35}$$

Substituting (10) into (35) and applying [29, Equation (72)], we obtain (36), shown at the top of the next page. Combining (35) and (36), we obtain T_2 as in (23), with

$$\begin{aligned} \Xi_{RD_1} &= \frac{[\eta_{v_{RD_1}}(1)]^2}{\eta_{v_{RD_1}}(2) - [\eta_{v_{RD_1}}(1)]^2}, \\ \Delta_{RD_1} &= \frac{\eta_{v_{RD_1}}(1)}{\eta_{v_{RD_1}}(2) - [\eta_{v_{RD_1}}(1)]^2}. \end{aligned} \tag{37}$$

Appendix B

The appendix B provides the detailed proof of theorem 2. From (20), we have

$$\begin{aligned} P_{D_2} &= \Pr\left(\min(\gamma_R^{x_1}, \gamma_R^{x_2}, \gamma_{D_2}^{x_1}, \gamma_{D_2}^{x_2}) < \gamma_{th}\right) \\ &= 1 - \Pr\left(\min(\gamma_R^{x_1}, \gamma_R^{x_2}, \gamma_{D_2}^{x_1}, \gamma_{D_2}^{x_2}) > \gamma_{th}\right) \\ &= \left[\begin{array}{l} 1 - \left(\Pr\left(\min(\gamma_R^{x_1}, \gamma_R^{x_2}) > \gamma_{th}\right)\right) \\ \times \left(\Pr\left(\min(\gamma_{D_2}^{x_1}, \gamma_{D_2}^{x_2}) > \gamma_{th}\right)\right) \end{array}\right] \\ &= 1 - \Big(1 - \Pr(\gamma_R < \gamma_{th})\Big)\Big(1 - \Pr(\gamma_{D_2} < \gamma_{th})\Big) \\ &= \Pr(\gamma_R < \gamma_{th}) + \Pr(\gamma_{D_2} < \gamma_{th}) \\ &- \Pr(\gamma_R < \gamma_{th}) \times \Pr(\gamma_{D_2} < \gamma_{th}) \\ &= T_3 + T_4 - T_3 \times T_4, \end{aligned} \tag{38}$$

where $\gamma_R = \min(\gamma_R^{x_1}, \gamma_R^{x_2})$ and $\gamma_{D_2} = \min(\gamma_{D_2}^{x_1}, \gamma_{D_2}^{x_2})$. Next, we can write

$$T_3 = \Pr(\gamma_R < \gamma_{th}) = \Pr\left(\min(\gamma_R^{x_1}, \gamma_R^{x_2}) < \gamma_{th}\right). \tag{39}$$

Because $\gamma_R^{x_1}, \gamma_R^{x_2}$ are two dependent random variables, substituting (5) and (6) into the formula (40), we can express T_3 as in (40) at the top of the next page.

We can see if $a_1 - a_2\gamma_{th} < 0$ then $T_3 = 1$. On the other hand, if $0 < a_1 - a_2\gamma_{th} \le a_2$, we have

$$\begin{aligned} T_3 &= \Pr\left((a_1 - a_2\gamma_{th})(Q_{SR}^{\max})^2 \Lambda X < \gamma_{th}\right) \\ &= \Pr\left(X < \frac{\gamma_{th}}{(a_1 - a_2\gamma_{th})(Q_{SR}^{\max})^2 \Lambda}\right). \end{aligned} \tag{41}$$

Setting $B = \dfrac{\gamma_{th}}{(a_1 - a_2\gamma_{th})(Q_{SR}^{\max})^2 \Lambda}$ and $\zeta_B = \frac{B\pi}{2M}\left(\frac{2ab}{2ab+\Omega}\right)^a$; similar as (34), we have

$$\begin{aligned} T_3 = \zeta_B \sum_{m=1}^{M} \frac{\sqrt{1-\phi_m^2}}{2b} \exp\left(-\frac{B}{4b}(1+\phi_m)\right) \\ \times {}_1F_1\left(a, 1, \frac{\Omega B(1+\phi_m)}{4b(2ab+\Omega)}\right). \end{aligned} \tag{42}$$

Another, if $a_1 - a_2\gamma_{th} > a_2$, we have

$$T_3 = \Pr(a_2 \Lambda X < \gamma_{th}) = \Pr(X < \frac{\gamma_{th}}{a_2 \Lambda}). \tag{43}$$

$$F_{v_{\mathrm{RD}_1}}\left(\sqrt{\frac{\gamma_{th}}{\mu\Lambda(b_1-b_2\gamma_{th})}}\right)=\frac{1}{\Gamma(\Xi_{\mathrm{RD}_1})}\gamma\left(\Xi_{\mathrm{RD}_1},\Delta_{\mathrm{RD}_1}\sqrt{\frac{\gamma_{th}}{\mu\Lambda(b_1-b_2\gamma_{th})}}\right)$$
$$=1-\frac{1}{\Gamma(\Xi_{\mathrm{RD}_1})}\Gamma\left(\Xi_{\mathrm{RD}_1},\Delta_{\mathrm{RD}_1}\sqrt{\frac{\gamma_{th}}{\mu\Lambda(b_1-b_2\gamma_{th})}}\right). \quad (36)$$

$$T_3=\Pr\left(\min(\gamma_{\mathrm{R}}^{x_1},\gamma_{\mathrm{R}}^{x_2})<\gamma_{th}\right)=\Pr\left(\min\left(\frac{\Lambda a_1(Q_{\mathrm{SR}}^{\max})^2X}{\Lambda a_2Q_{\mathrm{SR}}^{\max}X+1},\Lambda a_2(Q_{\mathrm{SR}}^{\max})^2X\right)<\gamma_{th}\right)$$
$$=\Pr\left(\min\left((a_1-a_2\gamma_{th})(Q_{\mathrm{SR}}^{\max})^2\Lambda X,a_2(Q_{\mathrm{SR}}^{\max})^2\Lambda X\right)<\gamma_{th}\right)$$
$$=\begin{cases}\Pr\left((a_1-a_2\gamma_{th})(Q_{\mathrm{SR}}^{\max})^2\Lambda X<\gamma_{th}\right), & (a_1-a_2\gamma_{th})\le a_2,\\ \Pr\left(a_2(Q_{\mathrm{SR}}^{\max})^2\Lambda X<\gamma_{th}\right), & (a_1-a_2\gamma_{th})>a_2.\end{cases} \quad (40)$$

Setting $C=\dfrac{\gamma_{th}}{a_2(Q_{\mathrm{SR}}^{\max})^2\Lambda}$ and $\zeta_C=\dfrac{C\pi}{2M}(\dfrac{2ab}{2ab+\Omega})^a$. By similar transformations as (42), we have:

$$T_3=\zeta_C\sum_{m=1}^{M}\frac{\sqrt{1-\phi_m^2}}{2b}\exp(-\frac{C}{4b}(1+\phi_m))$$
$$\times_1 F_1(a,1,\frac{\Omega C(1+\phi_m)}{4b(2ab+\Omega)}). \quad (44)$$

From formulas (42) and (44), we have (25). In addition to that, according to the DF operation, we have

$$T_4=\Pr(\gamma_{\mathrm{D}_2}<\gamma_{th})=\Pr\left(\min(\gamma_{\mathrm{D}_2}^{x_1},\gamma_{\mathrm{D}_2}^{x_2})<\gamma_{th}\right)$$
$$=\Pr\left(\min\left((b_1-b_2\gamma_{th})\mu\Lambda v_{\mathrm{RD}_2}^2,\mu\Lambda b_2v_{\mathrm{RD}_2}^2\right)<\gamma_{th}\right). \quad (45)$$

After similar transformations of (36), we obtain (46) (see the top of the next page). Applying transformation methods as in (35), we obtain T_4 as in (26), where

$$\Xi_{\mathrm{RD}_2}=\frac{[\eta_{v_{\mathrm{RD}_2}}(1)]^2}{\eta_{v_{\mathrm{RD}_2}}(2)-[\eta_{v_{RD_2}}(1)]^2},$$
$$\Delta_{\mathrm{RD}_2}=\frac{\eta_{v_{\mathrm{RD}_2}}(1)}{\eta_{v_{\mathrm{RD}_2}}(2)-[\eta_{v_{\mathrm{RD}_2}}(1)]^2}. \quad (47)$$

In (37) and (47), the $\eta_\Phi(t)$ is the tth moment of Φ, with $\Phi=\left(|v_{\mathrm{RD}_i}|,|h_{\mathrm{RD}_i}|,O_i,Z_i\right)$ and $O_i=|h_{\mathrm{RI}_n}||h_{\mathrm{I}_n\mathrm{D}_i}|, Z_i=\sum_{n=1}^{N}O_i$ is defined as follows

$$\eta_{|h_{\mathrm{RD}_i}|}(1)=\frac{\Gamma(m_{|h_{\mathrm{RD}_i}|}+\frac{1}{2})}{\Gamma(m_{|h_{\mathrm{RD}_i}|})}\sqrt{\frac{\Omega_{|h_{\mathrm{RD}_i}|}}{m_{|h_{\mathrm{RD}_i}|}}},$$
$$\eta_{|h_{\mathrm{RD}_i}|}(2)=\Omega_{|h_{\mathrm{RD}_i}|}, \quad (48)$$

and

$$\eta_{O_i}(t)=\left(\sqrt{\frac{m_{|h_{\mathrm{RI}_n}|}m_{|h_{\mathrm{I}_n\mathrm{D}_i}|}}{\Omega_{|h_{\mathrm{RI}_n}|}\Omega_{|h_{\mathrm{I}_n\mathrm{D}_i}|}}}\right)^{-t/2}$$
$$\times\frac{\Gamma(m_{|h_{\mathrm{RI}_n}|}+\frac{1}{2})\Gamma(m_{|h_{\mathrm{I}_n\mathrm{D}_i}|}+\frac{t}{2})}{\Gamma(m_{|h_{\mathrm{RI}_n}|})\Gamma(m_{|h_{\mathrm{I}_n\mathrm{D}_i}|})}. \quad (49)$$

Set

$$\eta_{Z_i}(1)=\sum_{n=1}^{N}\eta_{\mathrm{O}_i}(1), \quad (50)$$

$$\eta_{Z_i}(2)=\sum_{n=1}^{N}\eta_{\mathrm{O}_i}(2)+2\sum_{n=1}^{N}\sum_{n'=n+1}^{N}\left[\eta_{\mathrm{O}_i}(1)\right]^2, \quad (51)$$

and

$$\eta_{v_{\mathrm{RD}_i}}(1)=\eta_{|h_{\mathrm{RD}_i}|}(1)+\eta_{Z_i}(1), \quad (52)$$

$$\eta_{v_{\mathrm{RD}_i}}(2)=\eta_{|h_{\mathrm{RD}_i}|}(2)+\eta_{Z_i}(2)+2\eta_{|h_{\mathrm{RD}i}|}(1)\eta_{Z_i}(1). \quad (53)$$

References

[1] T. Q. Duong, L. D. Nguyen, T. T. Bui, K. D. Pham, and G. K. Karagiannidis, "Machine learning-aided real-time optimized multibeam for 6G integrated satellite-terrestrial networks: Global coverage for mobile services," *IEEE Network*, vol. 37, no. 2, pp. 86–93, Mar. 2023.

[2] J. Zhao, S. Li, X. Xu, H. Yan, and Z. Zhang, "Adaptive resource allocation of secured access to intelligent surface enhanced satellite–terrestrial networks with two directional traffics," *AEÜ - International Journal of Electronics and Communications*, vol. 170, p. 154746, Oct. 2023.

[3] S. Q. Nguyen, V. H. Nguyen, T. D. Tran, L. N. Nguyen, and L.-T. Tu, "On the security and reliability trade-off of the satellite terrestrial networks with fountain codes and friendly jamming," *EAI Endorsed Transactions on Industrial Networks and Intelligent Systems*, vol. 10, no. 4, p. e3, 2023.

[4] A. Guidotti, A. Vanelli-Coralli, M. Conti, S. Andrenacci, S. Chatzinotas, N. Maturo, B. Evans, A. Awoseyila, A. Ugolini, T. Foggi *et al.*, "Architectures and key technical challenges for 5G systems incorporating satellites," *IEEE Transactions on Vehicular Technology*, vol. 68, no. 3, pp. 2624–2639, Mar. 2019.

[5] S. Chen, S. Sun, and S. Kang, "System integration of terrestrial mobile communication and satellite communication—the trends, challenges and key technologies in B5G and 6G," *China Communications*, vol. 17, no. 12, pp. 156–171, Dec. 2020.

[6] G. Gür, "Spectrum sharing and content-centric operation for 5G hybrid satellite networks: Prospects and challenges for space-terrestrial system integration," *IEEE Vehicular Technology Magazine*, vol. 14, no. 4, pp. 38–48, Dec. 2019.

[7] N.-L. Nguyen, H.-N. Nguyen, A.-T. Le, D.-T. Do, and M. Voznak, "On performance analysis of NOMA-aided

$$T_4 = \begin{cases} 1; \frac{b_1}{b_2} < \gamma_{th} \\ \Pr(\mu\Lambda b_2 v_{\mathrm{RD}_2}^2 < \gamma_{th}); \frac{b_1}{b_2} > \gamma_{th} \geq \frac{b_1 - b_2}{b_2} \\ \Pr((b_1 - b_2\gamma_{th})\mu\Lambda v_{\mathrm{RD}_2}^2 < \gamma_{th}); \frac{b_1 - b_2}{b_2} > \gamma_{th} > 0 \end{cases} \quad (46)$$

hybrid satellite terrestrial relay with application in small-cell network," *IEEE Access*, vol. 8, pp. 188 526–188 537, Oct. 2020.

[8] L. Han, W.-P. Zhu, and M. Lin, "Outage of NOMA-based hybrid satellite-terrestrial multi-antenna DF relay networks," *IEEE Communications Letters*, vol. 10, no. 5, pp. 1083–1087, May 2021.

[9] L.Han, W.-P. Zhu, and M. Lin, "Outage analysis of multi-relay NOMA-based hybrid satellite-terrestrial relay networks," *IEEE Transactions on Vehicular Technology*, vol. 71, no. 6, pp. 6469–6487, Mar. 2022.

[10] R. Chai, L. Liu, F. Zou, J. Li, and Q. Chen, "Performance analysis of NOMA - based hybrid satellite-terrestrial relay networks with CCI," *IEEE Transactions on Network Science and Engineering*, vol. 10, pp. 2016–2029, Jan. 2023.

[11] L. Han, W.-P. Zhu, and M. Lin, "Uplink outage performance of NOMA-based hybrid satellite-terrestrial relay networks over generalized inhomogeneous fading channels," *IEEE Transactions on Communications*, vol. 70, no. 4, pp. 2417–2434, Jan. 2022.

[12] G. Xu, Z. Zhao, Z. Song, Q. Zhang, and B. Ai, "Symbol error analysis for integrated satellite-terrestrial relay networks with non-orthogonal multiple access under hardware impairments," *IEEE Transactions on Wireless Communications*, pp. 1–1, May 2024.

[13] X. Zhang, D. Guo, K. An, Z. Chen, B. Zhao, Y. Ni, and B. Zhang, "Performance analysis of NOMA-based cooperative spectrum sharing in hybrid satellite-terrestrial networks," *IEEE Access*, vol. 7, pp. 172 321–172 329, 2019.

[14] V. Singh and P. K. Upadhyay, "Exploiting FD/HD cooperative-NOMA in underlay cognitive hybrid satellite-terrestrial networks," *IEEE Transactions on Cognitive Communications & Networking*, vol. 8, no. 1, pp. 246–262, 2021.

[15] Z. Lin, H. Niu, K. An, Y. Wang, G. Zheng, S. Chatzinotas, and Y. Hu, "Refracting RIS-aided hybrid satellite-terrestrial relay networks: Joint beamforming design and optimization," *IEEE Transactions on Aerospace and Electronic Systems*, vol. 58, no. 4, pp. 3717–3724, Mar. 2022.

[16] Y. Ding, Y. Zou, and B. Li, "Ergodic Capacity and Outage Probability Analysis of RIS-Aided Hybrid Satellite-Terrestrial Networks," in *Proceedings of the 2022 14th International Conference on Wireless Communications and Signal Processing (WCSP)*. IEEE, Nov. 2022, pp. 837–841.

[17] K. Dolas and M. R. Bhatnagar, "On performance of IRS-assisted hybrid satellite–terrestrial cooperative communication," *IEEE Transactions on Aerospace and Electronic Systems*, vol. 59, no. 2, pp. 2020–2028, Apr. 2023.

[18] D. J. MacKay, "Fountain codes," *IEE Proceedings - Communications*, vol. 152, no. 6, pp. 1062–1068, Dec. 2005.

[19] A. Shokrollahi, "Raptor codes," *IEEE Transactions on Information Theory*, vol. 52, no. 6, pp. 2551–2567, Jun. 2006.

[20] D. MacKay, "Capacity approaching codes design and implementation," *IEE Proceedings - Communications*, vol. 152, no. 6, pp. 1060–1061, Jan. 2006.

[21] D. The Hung, T. Trung Duy, P. T. Tran, D. Quoc Trinh, and T. Hanh, "Performance comparison between fountain codes-based secure MIMO protocols with and without using non-orthogonal multiple access," *Entropy*, vol. 21, no. 10, p. 982, Oct. 2019.

[22] D. Hung, T. Duy, and D. Trinh, "Security-reliability analysis of multi-hop LEACH protocol with fountain codes and cooperative jamming," *EAI Endorsed Transactions on Industrial Networks and Intelligent Systems*, vol. 6, no. 18, p. 982, Mar. 2019.

[23] N.-L. Nguyen, L.-T. Tu, T. N. Nguyen, P.-L. T. Nguyen, and Q.-S. Nguyen, "Performance on cognitive broadcasting networks employing fountain codes and maximal ratio transmission," *Radioengineering*, vol. 32, no. 1, pp. 1–10, Dec. 2023.

[24] L.-T. Tu, T. N. Nguyen, P. T. Tran, T. T. Duy, and Q.-S. Nguyen, "Performance statistics of broadcasting networks with receiver diversity and fountain codes," *Journal of Information and Telecommunication*, vol. 7, no. 4, pp. 477–493, Jun. 2023.

[25] N. V. Toan, T. T. Duy, P. N. Son, D. T. Hung, N. Q. Sang, and L. T. Tu, "Outage performance of hybrid satellite-terrestrial relaying networks with rateless codes in co-channel interference environment," in *Proceedings of the 2023 International Conference on System Science and Engineering*. IEEE, Aug. 2023, pp. 468–473.

[26] P. M. Quang, N. Van Toan, T. T. Duy, and P. N. Son, "Performance Enhancement for Rateless Codes-Aided Hybrid Satellite-Terrestrial Multi-User Networks Using NOMA and IRS With Presence of Multiple Eavesdroppers," in *Proceedings of the 2024 IEEE International Conference on Consumer Electronics-Asia (ICCE-Asia)*, 2024, pp. 1–4.

[27] K. Guo, M. Lin, B. Zhang, J.-B. Wang, Y. Wu, W.-P. Zhu, and J. Cheng, "Performance analysis of hybrid satellite-terrestrial cooperative networks with relay selection," *IEEE Transactions on Vehicular Technology*, vol. 69, no. 8, pp. 9053–9067, Aug. 2020.

[28] A. Abdi, W. Lau, M.-S. Alouini, and M. Kaveh, "A new simple model for land mobile satellite channels: first- and second-order statistics," *IEEE Wireless Communications*, vol. 2, no. 3, pp. 519–528, May. 2003.

[29] B. C. Nguyen, N. T. Phuong, X. N. Tran, and P. T. Hiep, "On performance of RIS-aided ground-to-air and air-to-ground communications in multi-user NOMA systems," *Computer Networks*, vol. 228, p. 109754, Jun. 2023.

[30] D. L. Galappaththige, D. Kudathanthirige, and G. Amarasuriya, "Performance analysis of distributed intelligent reflective surface aided communications," in *Proceedings of the GLOBECOM 2020 - IEEE Global Communications Conference*. IEEE, Feb. 2020, pp. 1–6.

[31] I. Yildirim, A. Uyrus, and E. Basar, "Modeling and analysis of reconfigurable intelligent surfaces for indoor and outdoor applications in future wireless networks," *IEEE Transactions on Communications*, vol. 69, no. 2, pp. 1290–1301, Feb. 2021.

[32] M. Abramowitz and I. A. Stegun, *Handbook of mathematical functions with formulas, graphs, and mathematical tables*. US Government Printing Office, 1968, vol. 55.

Nguyen Van Toan received the B.S. degree in electrical engineering from Telecommunications University, Khanh Hoa, Vietnam, in 2007 and the M.S. degree in electrical engineering from the Posts and Telecommunications Institute of Technology (VNPT), Ho Chi Minh City, Vietnam, in 2013. Now, he is working toward the Ph.D. degree in the Faculty of Electrical and Electronics Engineering with Ho Chi Minh City University of Technology and Education (HCMUTE). His major research interests include hybrid satellite terrestrial relaying networks, cooperative communication, intelligent reflecting surfaces, fountain codes.

Pham Ngoc Son received the B.E. degree (2005) and M.Eng. degree (2009) in Electronics and Telecommunications Engineering from the Post and Telecommunications Institute of Technology, Ho Chi Minh City and Ho Chi Minh City University of Technology, Vietnam, respectively. In 2015, he received the PhD degree in Electrical Engineering from University of Ulsan, South Korea. He is currently an associate Professor in the Faculty of Electrical and Electronics Engineering (FEEE) of Ho Chi Minh City University of Technology and Education (HCMUTE). His major research interests are cooperative communications and cognitive radio, physical layer security, energy harvesting, intelligent reflecting surfaces, short packet communications, and deep learning.

Tran Trung Duy received the Ph.D. degree (2013) in electrical engineering from University of Ulsan, South Korea. From 2013 to the present, he joined the Posts and Telecommunications Institute of Technology (PTIT), Ho Chi Minh City campus. From 2017, he served as an associate editor of Transactions on Industrial Networks and Intelligent Systems. From 2021, he served as an associate editor of Hindawi Wireless Communications and Mobile Computing and Frontiers in Communications and Networks. His major research interests are cooperative communications, cooperative multi-hop, cognitive radio, physical-layer security, energy harvesting, hardware impairments, and fountain codes.

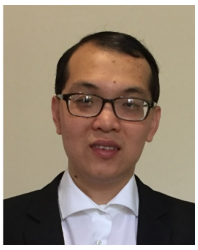

Lam-Thanh TU received the Ph.D. degree from the University of Paris Sud, Paris-Saclay University, France, in 2018. From 2022, he has been with the Faculty of Electrical and Electronics Engineering, Ton Duc Thang University, Vietnam. He has been a member of the Technical Program Committee of several conferences such as IEEE Globecom, IEEE ICC, IEEE SPAWC, EuCNC, IEEE ATC, and IEEE NICS, etc. His research interests include stochastic geometry, LoRa networks, reconfigurable intelligent surfaces, covert communications, and artificial intelligence applications for wireless communications.

Ta Van-Thanh received a B.S. degree in Telecommunication technological command from the Military Communication Officers' Training College (Vietnam) in 2010. He obtained the master's degree in Telecommunication Engineering from the Post and Telecommunications Institute of Technology (Vietnam) in 2014, and the Ph.D. degree in Electronic Engineering at Le Quy Don Technical University (LQDTU) in 2022. His research interests include digital systems, signal processing, high-speed hardware implementation, radio communication, and AI. Currently, he is a lecturer at the Faculty of Radio Communications, Telecommunications University (TCU), Vietnam.